行政院國家科學委員會補助專題研究計畫期中報告

一個平行化耦合 DSMC-NS 模擬程式的精進與通用化及其應用之研究(三年)

Improvement and Generalization of a Parallelized Hybrid DSMC-NS Code and Its Applications (3 Year)

計畫類別：☑個別型計畫　　□整合型計畫

計畫編號：NSC-96-2628-E-009-136-MY3

執行期間：96 年 08 月 01 日至 99 年 07 月 31 日

計畫主持人：吳宗信

共同主持人： 陳彥升

計畫參與人員：洪捷粲、許哲維

本成果報告包括以下應繳交之附件：

□ 赴國外出差或研習心得報告一份

□赴大陸地區出差或研習心得報告一份

□出席國際學術會議心得報告及發表之論文各一份

□國際合作研究計畫國外研究報告書一份

執行單位：國立交通大學機械工程學系

中　華　民　國　　98　年　05　月　30

行政院國家科學委員會專題研究計畫期中報告

一個平行化耦合 DSMC-NS 模擬程式的精進與通用化及其應用之研究(第二年)

Improvement and Generalization of a Parallelized Hybrid DSMC-NS Code and Its Applications (Second Year)

計畫編號：NSC-96-2628-E-009-136-MY3
執行期限：97 年 08 月 01 日至 98 年 07 月 31 日
主持人：吳宗信　國立交通大學機械工程學系
共同主持人：陳彥升 財團法人國家實驗研究院國家太空中心
計畫參與人員：洪捷粲、許哲維

中文摘要

許多重要問題的流場通常包含連續流體與稀薄氣體的區域. 對於這些問題的數值模擬無法僅考慮單一連續流體或分子動力學的方法來解決. 同時包含連續流體與分子動力學的複合法通常可用來解決這樣的問題. 在這三年的計畫裡, 我們將改進先前所發展的平行化複合直接模擬蒙地卡羅-那威爾史托克法的程式. 在第二年的計畫中, 我們利用 NS solver 進行 ramjet 及 scramjet 進氣口附近化學反應氣流場模擬. 同時發展及驗証一個針對非結構性網格的新型 mesh refinement 方法-virtual mesh refinement (VMR)以改善 DSMC solver 解析的準確度. 在此報告中將針對上述兩項研究進行報告.

關鍵字: 平行化直接模擬蒙地卡羅法, 複合直接模擬蒙地卡羅-那威爾史托克法, VMR, scramjet.

Abstract

Several important flow problems often involve continuum and rarefied regions in the flow fields. Numerical simulations of these flows can not be done properly alone using either continuum or particle method. Hybrid of continuum and particle methods is often required to properly resolve the flow fields. In this 3-year project, we proposed to refine and improve our previously developed parallelized hybrid DSMC-NS code. In the first year, we have converted the 3-D PDSC (Parallelized Direct Simulation Monte Carlo Code) into a general-purpose DSMC which features 2-D, 2-D axisymmetric and 3-D functionalities. In the second year, we have applied the NS equation solver to solve for chemical reacting flow field near the typical ramjet and scarmjet. In addition, we have also developed and validated a new mesh refinement, named virtual mesh refinement, for unstructured grids. Some issues related to these are discussed in this report.

Keywords: parallelized DSMC, hybrid DSMC-NS code, virtual mesh refinement.

1. Introduction

Several technically important flow problems often involve continuum and rarefied regions in the flow fields. Examples include expanding reaction control system plumes from a space vehicle[2,3], hypersonic flows past a blunt body[4], expanding plumes from a rocket at high altitude[5], high compression ratio turbomolecular pump[6] and jet-type chemical vapor deposition[7], to name a few. Unfortunately, neither continuum nor rarefied flow solver can be used alone to accurately and efficiently solve the entire flow field. Thus, how to efficiently and accurately simulate this kind of flows represents a great challenge to the computational fluid dynamics community at large.

Prior studies in solving flow fields involving continuum and rarified regions employed the hybrid DSMC-NS schemes with various approaches of coupling the particle and continuum methods. Detailed reviews of these approaches can be found in Schwartzentruber and Boyd[8-9] and Wu, *et al.*[1] and references cited therein. In general, a hybrid DSMC-NS method applies the concept of spatial domain decomposition to distinguish the computational domain of rarefaction or thermal non-equilibrium to

be modeled by the DSMC method, and the computational domain of continuum to be solved by the CFD (NS, Euler or Stokes) solver. Success of such hybrid numerical method relies upon four important issues[1]: 1) Accurate and efficient method in determining the breakdown region; 2) Proper and efficient flow properties exchange at breakdown interface; 3) The effect of steadiness of the flow solution on designing data exchange at the interface; 4) Proper detection of coupling convergence. In the present paper, we focus on the first and fourth issues that can further improve the efficiency of the hybrid DSMC-NS algorithm.

Wu, *et al.*[1] has developed a parallelized hybrid DSMC-NS scheme with unstructured grids, in which a continuum breakdown parameter[10] (Kn_{max}= max[Kn_D, Kn_V, Kn_T]) where $Kn_Q=|\nabla Q|\times\lambda/Q$ and a thermal non-equilibrium indicator ($P_{Tne}=|(T_{tr}-T_{rot})/T_{tr}$) were used to determine the continuum and thermal equilibrium breakdown regions, respectively. A domain overlapping strategy, taking advantage of unstructured data format, with Dirichlet-Dirichlet type boundary conditions based on these two breakdown parameters is used iteratively to determine the choice of solvers in the spatial domain. These breakdown regions were simulated using the more expensive DSMC method, while other regions were simulated using the relatively cheaper NS equation solver. Normally, the size of the overlapping region is about 2-3 layers extending from the particle side towards continuum side to make sure the Maxwellian distribution can be applied accurately at solver-solver boundaries. Results showed that, not only the leading edge and shock, but also the boundary layer regions are identified as breakdown regions, in which large velocity gradient due to high-speed flows is often the dominating factor in determining Kn_{max}.

In brief summary, there are still several issues, which require further investigation. *First*, the inclusion of the boundary layer as the continuum breakdown region often caused slow convergence or even wrong solution of the coupling, which was also found by Schwartzentruber and Boyd[11]. Now question arises: is it truly continuum breakdown in the whole domain of boundary layer? *Second*, no automatic convergence mechanism of the coupling was tested, which is important in practice. Only constant number of iterations in both NS and DSMC were employed to obtain the final coupling solution. *Third*, the computational cost could be higher than the pure DSMC solution mainly due to the expensive DSMC simulations for several couplings. Any strategy of reducing the computational cost of DMSC should be highly welcome. This issue has been addressed by Schwartzentruber and Boyd[8-9] by using so-called "sub-relaxation" scheme in DSMC sampling and will not be discussed here. In this report, we intend to address the first two issues and hopefully we can improve the hybrid DSMC-NS algorithm to become a more practical tool in simulating flow field involving continuum and continuum/thermal equilibrium breakdown regions, such as hypersonic flows.

The present midterm report is organized as follows. Numerical methods are introduced briefly in Section 2, in which the NS equation solver and DSMC code are included. Section 3 presents the results of CFD simulation and validation of a virtual mesh refinement in PDSC. Finally, in Section 4, the conclusions of the present study are summarized along with several possible future directions of research.

2. Numerical methods

2-1. The NS equation solver

The CFD methodology is based on a multi-dimensional, finite-volume, viscous, chemically reacting, unstructured grid, and pressure-based formulation. Time-varying transport equations of continuity, species continuity, momentum, total enthalpy, turbulent kinetic energy, and turbulent kinetic energy dissipation were solved using a time-marching sub-iteration scheme and are written as:

$$\frac{\partial \rho}{\partial t}+\frac{\partial}{\partial x_j}\left(\rho u_j\right)=0 \tag{1}$$

$$\frac{\partial \rho\alpha_i}{\partial t}+\frac{\partial}{\partial x_j}\left(\rho u_j\alpha_j\right)=\frac{\partial}{\partial x_j}\left[\left(\rho D+\frac{\mu_t}{\sigma_\alpha}\right)\frac{\partial \alpha_i}{\partial x_j}\right]+\omega_i \tag{2}$$

$$\frac{\partial \rho u_i}{\partial t}+\frac{\partial}{\partial x_j}\left(\rho u_j u_i\right)=-\frac{\partial p}{\partial x_i}+\frac{\partial \tau_{ij}}{\partial x_j} \tag{3}$$

$$\frac{\partial \rho H}{\partial t}+\frac{\partial}{\partial x_j}\left(\rho u_j H\right)=\frac{\partial p}{\partial t}+Q_r+\frac{\partial}{\partial x_j}\left(\left(\frac{K}{C_p}+\frac{\mu_t}{\sigma_H}\right)\nabla H\right)+\frac{\partial}{\partial x_j}\left(\left(\left(\mu+\mu_t\right)-\left(\frac{K}{C_p}+\frac{\mu_t}{\sigma_H}\right)\right)\nabla\left(V^2/2\right)\right)+\theta \tag{4}$$

$$\frac{\partial \rho k}{\partial t}+\frac{\partial}{\partial x_j}\left(\rho u_j k\right)=\frac{\partial}{\partial x_j}\left[\left(\mu+\frac{\mu_t}{\sigma_k}\right)\frac{\partial k}{\partial x_j}\right]+\rho\left(\Pi-\varepsilon\right) \tag{5}$$

$$\frac{\partial \rho \varepsilon}{\partial t}+\frac{\partial}{\partial x_j}\left(\rho u_j \varepsilon\right)=\frac{\partial}{\partial x_j}\left[\left(\mu+\frac{\mu_t}{\sigma_\varepsilon}\right)\frac{\partial \varepsilon}{\partial x_j}\right]+\rho\frac{\varepsilon}{k}\left(C_1\Pi-C_2\varepsilon+C_3\Pi^2/\varepsilon\right) \tag{6}$$

A predictor plus corrector solution algorithm was employed to provide coupling of the governing equations. A second-order central-difference scheme was employed to discretize the diffusion fluxes and source terms. For the convective terms, a second-order upwind total variation diminishing difference scheme was used. To enhance the temporal accuracy, a second-order backward difference scheme was employed to discretize the temporal terms. Details of the numerical algorithm can be found in Ref's [12)-18)].

An extended k-ε turbulence model[19] was used to describe the turbulence. A modified wall function approach was employed to provide wall boundary layer solutions that are less sensitive to the near-wall grid spacing. Consequently, the model has combined the advantages of both the integrated-to-the-wall approach and the conventional law-of-the-wall approach by incorporating a complete velocity profile and a universal temperature profile[17]. A finite-rate chemistry chemical reaction mechanism[14)-20)] was

used to describe the combustion process occurs inside the scramjet combustion chamber.

In the present numerical investigation, hydrogen/air combustion conditions are of interest. A reduced 9-step hydrogen/oxygen reaction chemical kinetics mechanism [12)-13)] is employed for the combustion simulation. This chemistry model is summarized in Table 1.

2-2. DSMC method

The direct simulation Monte Carlo (DSMC) method is a computational tool for simulating flows in which effects at the molecular scale become significant[1)]. The Boltzmann equation, which is appropriate for modelling these rarefied flows, is extremely difficult to solve numerically due to its high dimensionality and the complexity of the collision term. DSMC provides a particle based alternative for obtaining realistic numerical solutions.

In this report, a new mesh-refining process (virtual mesh refinement) for DSMC using unstructured grids, which is based on the TAS (transient adaptive sub-cell) concept, is introduced to virtually refine the background cells. Virtual mesh refinement (VMR) based on the data obtained on the initial DSMC simulation using the background grid. The results of the initial DSMC simulation are used to determine the local mean free path in each background cell, which is then compared with the corresponding cell size. The result of comparison is then used to calculate the number of refined cells in each coordinate direction required to resolve the local mean free path in background cell. Note the refined cell is organized as Cartesian structured grids with the same cell size. Refined cell size is normally taken to be less than one half of the local mean free path, although it can be controlled by the user. A typical example is schematically shown in **Figure 1**. One important advantage is the particle tracing becomes very efficient which results directly from the use of Cartesian structured grids for the refined cells. The sub-cell in each background cell, which contains the background cell centroid is also identified in this step. This will be used in the final data output.

In addition, area of each sub-cell ("area" in two-dimensional case; "volume" in three-dimensional case), which is geometrically inside the background cell, is calculated using the Monte Carlo (MC) method. Note the area of the sub-cell (or volume) is required in calculating the number of collision pairs such as NTC method[21)]. The reason not to apply the conventional method such as coordinate geometry is that it becomes very cumbersome and complicated as it is extended to three-dimensional case. The MC method is easy in concept as well as practical implementation, as shown schematically in **Figure 2.** Each particle with randomly assigned position is checked if it is located in the background cell. Once it is located in the background cell, then the sub-cell which contains the particle is easily determined by taking advantage of the Cartesian structured sub-cells. Only those particles located inside the sub-cell and background cell are counted for the area calculation. The area of the *i*th sub-cell inside the background cell is thus calculated as follows:

$$V_{vc_i} = V_c \times R_i / \sum_{i=1}^{N_{vc}} R_i$$

where *Ri* is the number of particles located inside the *ith* sub-cell, *Vc* is the area of background cell and *Nvc* is the total number of sub-cells. Our experience shows that approximately 5,000**Nvc* particles are required to reach 0.1% error for area calculations of all the sub-cells, which takes about 12.5 minutes of computational time for ~300,000 virtual sub-cells using 12 processors. This computational overhead is comparatively low as compared to the total DSMC simulation in general.

3. Results and Discussion

3.1 N-S equation solver

3.1.1. Ramjet Inlet Flow

The experimental study of an axisymmetric ramjet inlet flow was performed by Nagarathinam[22]. The half angle of the inlet spike is 20 degrees. The experimental test conditions are Mach 2.18 freestream, 296,000 Pa total pressure and 300 K total temperature. The strut that holds the center body to the cowl casing is omitted in the numerical computation.

To represent this model numerically, a mesh with 29,820 elements is generated (grid unit: 5 cm), which gives good grid resolution of the flow inside the inlet. The backpressure effect is provided using a porosity model, which represents the blockage effects in the flowfield downstream of the center body. A converged solution is obtained in 60,000 time steps with a 1.0E-06 sec time step size, which takes 60.6 minutes CPU time using 8 processors with 99 percent parallel efficiency. This solution takes longer to run due to the need to adjust the blockage porosity to match the backpressure of the experiment.

The predicted pressure field in the ramjet inlet is shown in **Fig. 3**, which indicates pressure recovery due to applied flow blockage effect downstream of the inlet that match the test conditions. **Fig. 4** illustrates the predicted Mach number distributions of the ramjet inlet. For supersonic flow computations, numerical accuracy is critical in order to keep numerical diffusion low so as not to affect the resolution of flow and shock structures.

3.1.2 Scramjet Inlet Flow

The experimental investigation of this test case was conducted by Yanta et al.[23] The inlet geometry consists of a forebody wedge angle of 10 degrees and

a 13-degree inward turning duct (inner wall turning radius of 0.057 m). The test conditions of this experiment are Mach 4 freestream, 101,350 Pa static pressure and 311 K static temperature.

A mesh with 36,580 cells is generated for numerical computation (grid unit: 10 cm), which gives good grid resolution of the flow inside the inlet. A converged solution is obtained in 10,000 time step with a 3.0E-06 sec time step size, which takes 15.2 minutes CPU time using 8 processors with 99.2 percent parallel efficiency.

The predicted scramjet inlet pressure field is shown in **Fig. 5**, which gives clear resolution of the shock train system in the inlet duct. Again, for supersonic flow calculations, numerical accuracy is critical such that minimum numerical diffusion can be kept for good flow structure resolution. As a part of the present numerical tests, a first-order upwind scheme was tried, which ends up with a false bow shock upstream of the cowl lip and destroy the shock structure in the inlet duct. **Fig. 6** shows the predicted temperature contours. A high temperature region is predicted along the bottom wall just downstream of the inlet turn. This is caused by cowl lip shock interaction with the bottom wall boundary layer that separates and forms a steady recirculation region where high temperature recovery occurs. This flow separation feature is also revealed in **Figs. 7** and **8** of Mach number contour plots. Similar flow phenomenon is also observed in the experiment. For scramjet inlet designs, the cowl lip shock strength should be controlled by geometry tailoring such that this flow separation phenomenon can be avoided.

3.2 DSMC method

We have developed a two-level virtual mesh refinement (VMR) method and implemented in the parallelized direct simulation Monte Carlo code (PDSC) which utilizes unstructured grids. The implementation was validated by simulating one hypersonic flow and compared the results with the benchmark solution. **Figure 9** shows the sketch of the Mach-15 hypersonic flow past a cylinder and related positions of presenting the profiles of properties, which is used for verification of the VMR implementation in PDSC. Important free-stream flow conditions include: argon gas, velocity of 3246 m/s, temperature of 135 K, number density of 1.41E21 m-3, Mach number of 15, and wall temperature of 300 K. Corresponding free-stream Knudsen number is 0.06 based on the free-stream mean free path ($\lambda\infty$=0.000981 m) and the diameter of the cylinder (D=0.3048 m).

Figure 10 shows the pressure distribution around the scramjet. The flow after the first oblique shock impinges on the upper leading edge, which causes reflected shock to interact with the boundary layer flow along the bottom ramp. Finally, the flow inside the horizontal channel becomes a typical channel flow and further expands to the ambient at the exit. The flow just behind the reflected shock near the upper channel wall becomes stagnant and thus high-pressure. The flow phenomena are reflected from **Figure 11** and **12**, which show the surface properties along the upper and lower channel wall, respectively. Results clearly show that the proposed VMR algorithm in PDSC can faithfully reproduce benchmark results with a much reduced cost up to 3-5 times.

4. Conclusion

In this year, we have: 1) applied the NS equation solver to simulate reacting flow field near the ramjet and scamjets and 2) developed and validated a VMR algorithm in PDSC. The former show that the present NS equation solver can predict importatnt features of these challenging supersonic to hypersonic flows. The latter show that the newly proposed VMR can faithfully reproduce the benchmark solution with a much reduced computational cost.

In the third year, we intend to combine these above two to simulate some challenging hypersonic flows and will be describe in detail in the final report.

References

1. Wu, J.-S., Lian, Y.-Y., Cheng, G., Koomullil, R. P. and Tseng, K.-C.: Development and Verification of a Coupled DSMC-NS Scheme Using Unstructured Mesh, *J. Comput. Phys*, **219** (2006), pp. 579-607.
2. Taniguchi, M., Mori, H., Nishihira, R. and Niimi, T.: Experimental analyses of flow field structures around clustered linear aerospike nozzles, *AIP Conference Proc.*, **762** (2005), pp. 349-354.
3. Ivanov, M. S., Khotyanovsky, D. V., Kudryavtsev, A. N., Vashchenkov, P. V., Markelov, G. N., Schmidt, A. A.: Numerical study of backflow for nozzle plumes expanding into vacuum, *AIAA Paper 2004-2687* (2004).
4. Moss, J. N., Price, J. M.: Survey of Blunt Body Flows including wakes at Hypersonic Low-Density Conditions, J. Thermophysics & Heat Transfer, Vol. 11, No. 3, pp. 321-329, 1997.
5. Wilmoth, Richard G., Yellin, Keith A. and Papp, John L.: Continuum-DSMC Coupling Issues for Steady and Unsteady Two-Phase Plumes, *28th EPTS and 10th SPIRITS User Group Joint Meeting*, San Diego, 2004.
6. Cheng, H.-P., Jou, R.-Y., Chen, F.-Z., and Chang, Y.-W.: Three-Dimensional Flow Analysis of Spiral-Grooved Turbo Booster Pump in Slip and Continuum Flow, *J. Vacu.*

Sci. Tech. A: Vacuum, Surface, and Films, **18** (1999), pp. 543-551.

7. Versteeg, V., Avedisian, C. T. and Raj, R.: Method and Apparatus for CVD Using Liquid Delivery System with an Ultrasonic Nozzle, *U.S Patent Number: 5,451,260* (1994).
8. Schwartzentruber, T. E., Boyd, I. D.: A hybrid particle-continuum method applied to shock waves, *J. Comput. Phys.*, **215** (2006), pp.402-416.
9. Schwartzentruber, T. E., Scalabrin, L. C. and Boyd, I. D.: A modular particle-continuum numerical method for hypersonic non-equilibrium gas flows, *J. Comput. Phys.*, **225** (2007), pp. 1159-1174.
10. Wang, W.-L. and Boyd, I. D.: Predicting Continuum Breakdown in Hypersonic Viscous Flows, *Physics of Fluids*, **15** (2003), pp. 91-100.
11. Schwartzentruber, T. E., Scalabrin, L. C. and Boyd, I. D.: Progress on a Modular Particle-Continuum Numerical Method for Multi-Scale Hypersonic Flows, *DSMC Theory, Methods, and Applications Conference*, NM., 2007.
12. Wang, T.S., Chen, Y.S., "Unified Navier-Stokes Flowfield and Performance Analysis of Liquid Rocket Engines," *J. Propulsion and Power*, Vol. 9, No. 5, pp. 678-685, 1993.
13. Chen, Y.-S., Liu, J., Zhang, S., and Mallapragada, P., "An Integrated Tool for Launch Vehicle Base-Heating Analysis," Final Report, NAS8-00002, Engineering Sciences, Inc., Huntsville, AL, 2001.
14. Liaw, P., Shang, H.M., Chen, Y.S., "Particulate Multi-Phase Flowfield Calculation with Combustion/Breakup Models for Solid Rocket Motor," AIAA-94-2780, 30th AIAA/ASME/SAE/ASEE Joint Propulsion Conference, June 27-29, 1994, Indianapolis, IN.
15. Chen. Y.-S., Zhang S., and Liu, J., "Stage Separation Performance Analysis Project," Final Report, H-34345D, Engineering Sciences, Inc., Huntsville, AL, 2002.
16. Wang, T.-S., Chen, Y.-S., Liu, J., Myrabo, L.N., and Mead, F.B. Jr., "Advanced Performance Modeling of Experimental Laser Lightcraft," *Journal of Propulsion and Power,* Vol. 18, No. 6, 2002, pp. 1129-1138.
17. Wang, T.-S., "Multidimensional Unstructured-Grid Liquid Rocket Engine Nozzle Performance and Heat Transfer Analysis," *Journal of Propulsion and Power*, Vol. 22, No. 1, 2005, pp. 78-84.
18. Wang, T.-S., "Transient 3-D Analysis of Nozzle Side Load in Regeneratively Cooled Engines," AIAA Paper 2005-3942, 41st AIAA/ASME/SAE/ASEE Joint Propulsion Conference, Tucson, Arizona, 2005.
19. Chen, Y.-S., and Kim, S. W., "Computation of Turbulent Flows Using an Extended k-ε Turbulence Closure Model," NASA CR-179204, 1987.
20. Wang, T.-S., "Thermophysics Characterization of Kerosene Combustion," *Journal of Thermophysics and Heat Transfer*, Vol. 15, No. 2, 2001, pp.140-147.
21. G.A. Bird, *Molecular Gas Dynamics and the Direct Simulation of Gas Flows*, Oxford University Press, 1994.
22. Nagarathinam, M., Gupta, A., and Davidson, D., "Wind Tunnel Testing of Axisymmetric Air Intake," Technical Report, DRDL, 5120.1003.000, NAL, 1985.
23. Yanta, W.J., Collier, A.S., Spring, C. III, Boyd, W., Christopher, F., and McArthur, J.C., "Experimental Measurements of the Flow in a Scramjet Inlet at Mach 4," *J. of Propulsion*, Vol. 6, No. 6, p. 784-790, 1990.

Equation	A	N	E/R
$O_2 + H_2 = 2\ OH$	1.700E+13	0	24233
$H_2 + OH = H_2O + H$	2.190E+13	0	2590
$2\ OH = H_2O + O$	6.023E+12	0	550
$H_2 + O = H + OH$	1.800E+10	1	4480
$O_2 + H = O + OH$	1.220E+17	-0.91	8369
$O + H + (M) = OH + (M)$	1.000E+16	0	0
$2\ O + (M) = O_2 + (M)$	2.550E+18	-1	59390
$2\ H + (M) = H_2 + (M)$	5.000E+15	0	0
$H + OH + (M) = H_2O + (M)$	8.400E+21	-2	0

Table 1. Hydrogen/oxygen chemical kinetics in Arrhenius form, $k = A\ T^N\ e^{-E/RT}$.

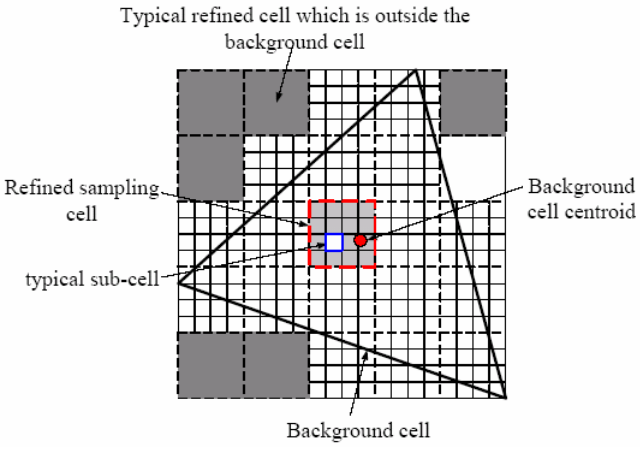

FIGURE 1. Typical refined cells (dashed lines) on a triangular background cell (solid lines) along with TAS.

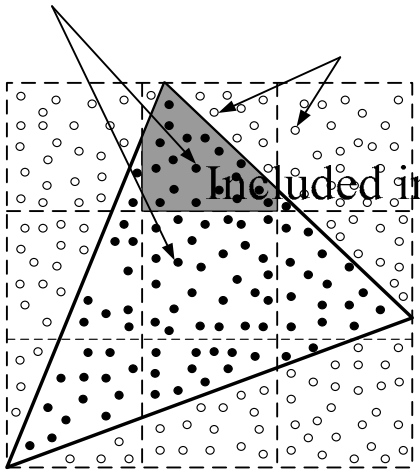

FIGURE 2. Sketch of calculating the sub-cell area inside an unstructured background cell using Monte Carlo method.

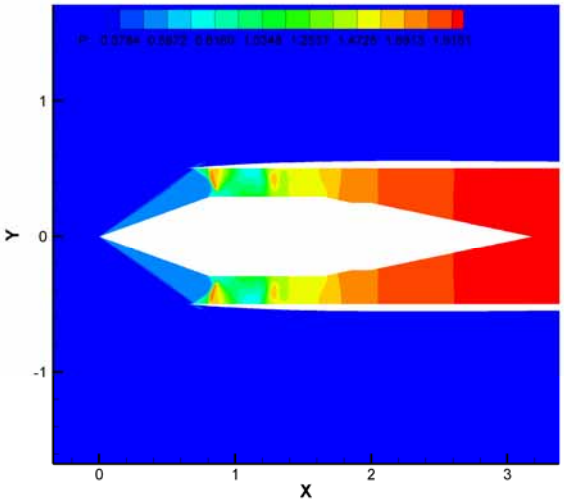

FIGURE 3. Predicted ramjet inlet pressure contours.

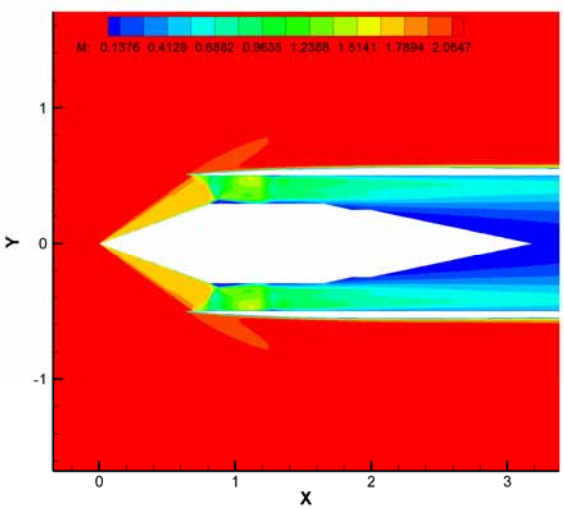

FIGURE 4. Predicted ramjet inlet Mach contours.

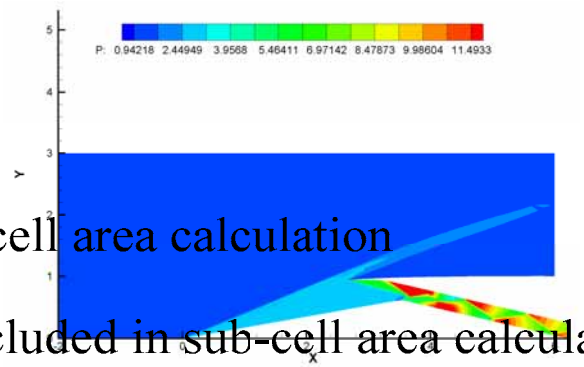

FIGURE 5. Scramjet inlet pressure contours.

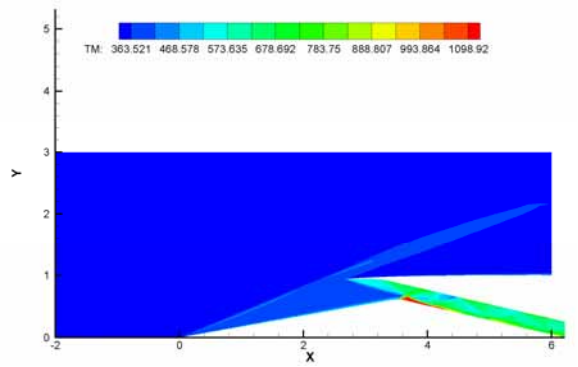

FIGURE 6. Scramjet inlet temperature contours.

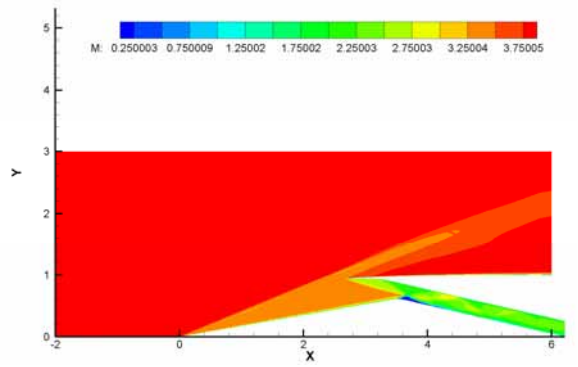

FIGURE 7. Predicted inlet Mach number contours.

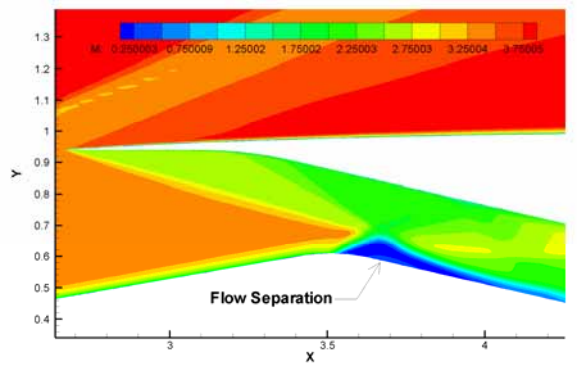

FIGURE 8. Flow solution showing inlet separation.

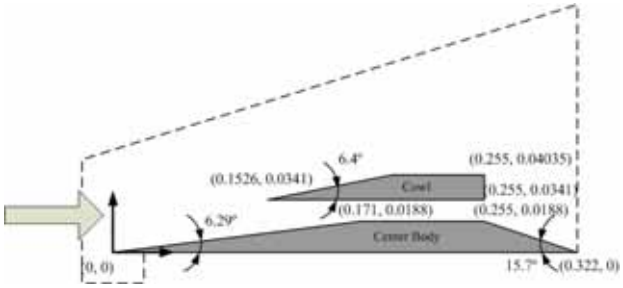

FIGURE 9. Sketch of a scramjet flow.

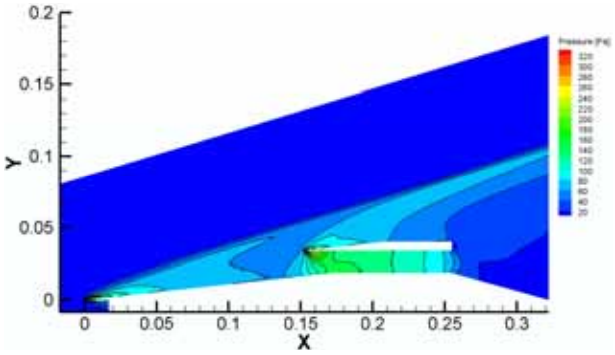

FIGURE 10. Pressure contour of a M-15 scramjet flow.

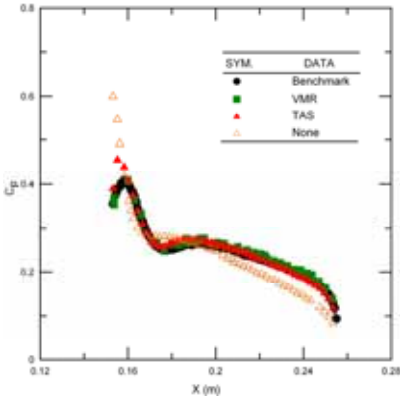

(a)

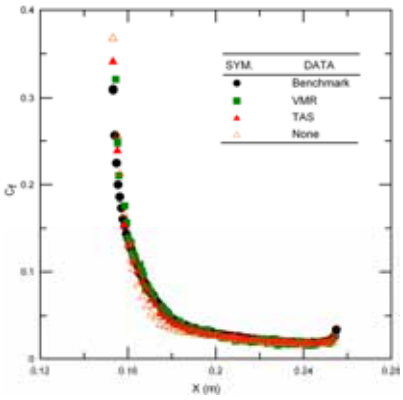

(b)

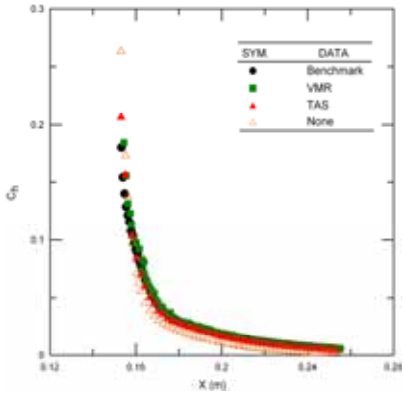

(c)

FIGURE 11. Surface property distribution along the top channel wall. (**a**) local pressure coefficient. (**b**) local friction coefficient. (**c**) local heat transfer coefficient.

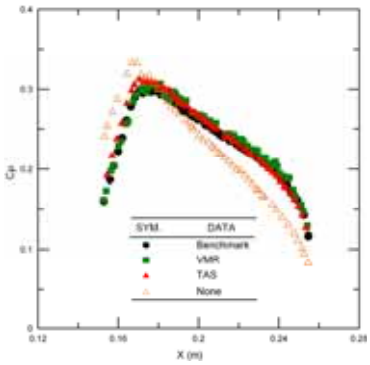

(a)

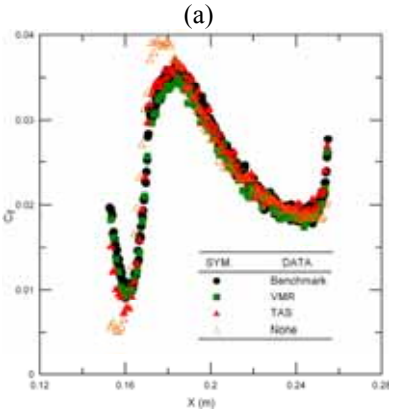

(b)

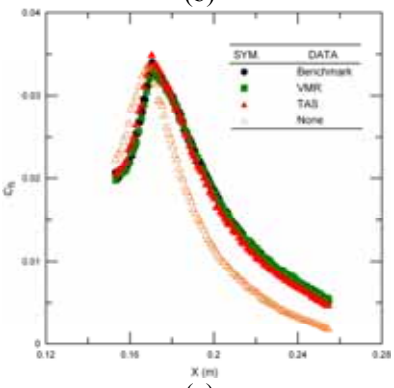

(c)

FIGURE 12. Surface property distribution along the bottom channel wall. (**a**) local pressure coefficient. (**b**) local friction coefficient. (**c**) local heat transfer coefficient.